JOURNAL OF MAGNETIC RESONANCE **134,** 57–66 (1998)
ARTICLE NO. MN981526

Simulation Methods for Looping Transitions

Betty J. Gaffney* and Harris J. Silverstone†

*National High Magnetic Field Laboratory and Institute for Molecular Biophysics, Florida State University, 1800 East Paul Dirac Drive, Tallahassee, Florida 32310; and †Department of Chemistry, The Johns Hopkins University, 3400 North Charles Street, Baltimore, Maryland 21218

E-mail: bgaffney@magnet.fsu.edu

Received February 27, 1998; revised May 20, 1998

Looping transitions occur in field-swept electron magnetic resonance spectra near avoided crossings and involve a single pair of energy levels that are in resonance at two magnetic field strengths, before and after the avoided crossing. When the distance between the two resonances approaches a linewidth, the usual simulation of the spectra, which results from a linear approximation of the dependence of the transition frequency on magnetic field, breaks down. A cubic approximation to the transition frequency, which can be obtained from the two resonance fields and the field-derivatives of the transition frequencies, along with linear (or better) interpolation of the transition-probability factor, restores accurate simulation. The difference is crucial for accurate line shapes at fixed angles, as in an oriented single crystal, but the difference turns out to be a smaller change in relative intensity for a powder spectrum. Spin-$\frac{3}{2}$ Cr^{3+} in ruby and spin-$\frac{5}{2}$ Fe^{3+} in transferrin oxalate are treated as examples. © 1998 Academic Press

Key Words: **simulation of $S > 1$; looping transition; chromium ion; iron ion; transferrin.**

INTRODUCTION

A "looping transition" occurs in field-swept electron magnetic resonance (EMR) spectra of $S > \frac{1}{2}$ systems at fields and molecular orientations where energy levels have avoided crossings: a given pair of energy levels is in resonance at two separate magnetic fields, before and after the (avoided) crossing. A plot of the two resonance fields as a function of the orientational angles is typically U-shaped or, in some cases, a closed oval. Figure 1 displays a looping transition in ruby.

When the separation between the two resonance fields of a looping transition is within a few linewidths (in Fig. 1, when θ is close to 30°), accurate simulation of the lineshape becomes complicated. We present here a simple computational solution for calculating EMR spectra for looping transitions. The key idea is to approximate the highly non-linear difference between the two energy levels as a cubic polynomial in the magnetic field by using four constants already calculated in determining the resonance fields (*1, 2*).

Looping transitions have been studied experimentally and theoretically in depth by Pilbrow *et al.* (*3*) and by Wang and Pilbrow (*4*) for $S = \frac{3}{2}$ systems. In the EMR of a ruby single crystal at 9.521 GHz, looping transitions are important when the angle between the c axis and the magnetic field is near 30° and near 89°. Pilbrow *et al.* (*3*) were especially concerned with the asymmetry in width and intensity of the two companion resonances when close together. They simulated the field-swept EMR spectra by computing, field-point by field-point, the transition frequencies $\nu(B)$ and corresponding squared transition-dipole matrix elements $|V_{ij}(B)|^2$ for use in the (frequency-swept) formula for the spectral response function $S(B)$,

$$S(B) = C'|V_{ij}(B)|^2 f(\nu(B) - \nu_0, \sigma_\nu). \qquad [1]$$

Here $f(\nu - \nu_0, \sigma_\nu)$ is a (frequency-swept) lineshape function centered at the spectrometer operating frequency ν_0, and σ_ν is the linewidth in the frequency domain. [Notation difference: we use ν_0 where Pilbrow *et al.* (*3*) use ν_c, and we use $\nu(B)$ where they use $\nu_0(B)$.]

At each field strength the calculation of $\nu(B)$ and $|V_{ij}(B)|^2$ requires a matrix diagonalization. In a powder simulation, where the calculational effort is multiplied by the number of orientations and the number of field points, Eq. [1] is often simplified by assuming that the transition frequency varies linearly with the magnetic field near resonance, $\nu(B) - \nu_0 \sim (B - B_0)b$, and that the transition-dipole is constant, to obtain an equivalent, but approximate, field-swept lineshape function valid near B_0:

$$S(B) \sim C'|V_{ij}(B_0)|^2 f((B - B_0)b, \sigma_\nu). \qquad [2]$$

Here b is a constant, and the resonance field B_0 is where $\nu_0 = \nu(B_0)$. The considerations for making the frequency-to-field conversion were discussed by Aasa and Vänngard (*5*) and by Pilbrow (*6*). In the simplest case, the separation of the energy levels near a transition is a linear function of magnetic field, so that the field-normalized intensity of the lineshape is inversely proportional to the effective g factor. More generally, the field-normalized intensity is inversely proportional to $|b| = |d\nu(B_0)/dB_0|$, the derivative with respect to field of the sepa-

1090-7807/98 $25.00

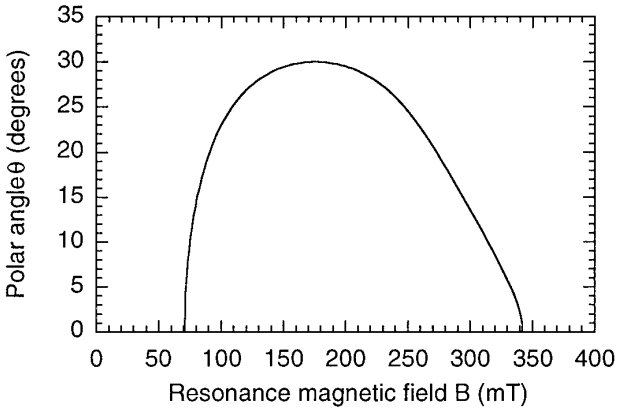

FIG. 1. Resonance magnetic field versus polar angle for a typical looping transition in ruby. See text for details.

ration of energy levels between which transition occurs (*5*). Neither of these approximations is accurate at a looping transition.

EMR spectra provide many other examples, besides that of ruby, of looping transitions in well-studied samples. Some of these examples include the $S = \frac{5}{2}$ systems, oriented single crystals of sodium- or lithium-compensated ferric centers in α-quartz (*7, 8*), and an $S = \frac{3}{2}$ example, alkali halide doped with $Cr(CN)_6^{3-}$ (*9*). In biological samples, interdoublet transitions in EMR of $S = \frac{5}{2}$ systems provide examples of looping transitions when the applied microwave frequency is in the range of 1 to 4 times the zero-field splitting parameter D. This condition is found in X-band EMR of high-spin ferric transferrin (*10, 11*) and in W-band simulations with parameters characteristic of ferric lipoxygenase (*12*). To illustrate applications of the cubic polynomial approach to converting frequency-swept lineshapes to field-swept ones, we first revisit the ruby example of Pilbrow *et al.* and then apply the technique to simulations of the X-band EMR spectra relevant to transferrin oxalate.

HOW THE LINEAR APPROXIMATION FAILS NEAR A LOOPING POINT: $S = \frac{3}{2}$, AXIALLY SYMMETRIC CASE

To derive an approximate field-swept lineshape function is to replace the right-hand side of Eq. [1] with an expression explicitly simple in its dependence on $B - B_0$ and accurate. To illustrate the problem and its solution, we borrow the ruby case discussed by Pilbrow *et al.* (*3*), which (i) provides a good experimental example of a looping transition in single crystal studies, and which (ii) is relatively simple. The ruby crystal contains two magnetic $S = \frac{3}{2}$ Cr^{3+} impurity sites related by inversion and has the axially symmetric spin-Hamiltonian (*3*),

$$\hat{H} = \beta[g_{\parallel}S_zB_z + g_{\perp}(S_xB_x + S_yB_y)] + D(S_z^2 - \tfrac{1}{3}\mathbf{S}^2). \quad [3]$$

The experimental parameters (*3*) (with uncertainties omitted) are $g_{\parallel} = 1.9840$, $g_{\perp} = 1.9867$, and $D = -5.747$ GHz $= -0.191699$ cm^{-1}. Following Ref. (*3*), we replace $g_{\parallel}$ and $g_{\perp}$ by an isotropic average $g = 1.9858$. The energy levels of Eq. [3] are easily obtained by diagonalizing a 4×4 matrix.

Pilbrow *et al.* (*3*) showed that when the angle θ between the magnetic field and the crystal c axis (z axis in Eq. [3]) was near 30° or 89°, the two branches of looping transitions are seen in a magnetic field range that is a small multiple of the apparent linewidth. We discuss here the 30° case, which we have already visited in Fig. 1, where the coalescence and disappearance of the looping transition near 30° is apparent. We set $\theta = 29.4°$ and plot in Fig. 2 the four energy levels as B increases from 0 to 500 mT. Notice that the two middle levels, labeled by 2 and 3 in the figure, undergo an avoided crossing near $B = 200$ mT. The experimentally observed looping transition links Level 2 with Level 4 and takes place at a frequency of 9.521 GHz $= 0.317586$ cm^{-1}. The inset in Fig. 2 shows how the energy separation between these two levels passes through resonance first near 150 mT and a second time near 200 mT. (In high magnetic field, Level 4 has $m_s = +\frac{3}{2}$, while Level 2 has $m_s = -\frac{1}{2}$.)

Next we plot in Fig. 3 the field-swept EMR spectrum for $\theta = 29.4°$. The dots are an "exact" application of Eq. [1] with B running from 120 to 225 mT in steps of 1 mT. The dot spectrum can be compared to Fig. 2a of Ref. (*3*). The dashed line in Fig. 3 is the result of using the usual "linear approximation" for $\nu(B)$ at each of the two resonance fields, Eq. [2], twice. The fit is not bad, but shows discrepancies between the two resonances that get worse as θ increases (see below).

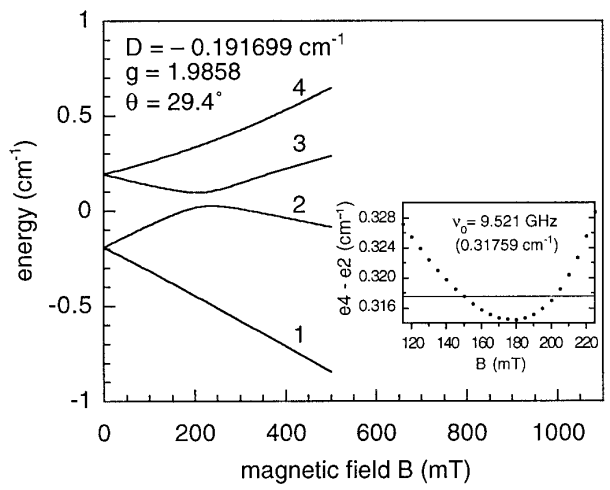

FIG. 2. The magnetic-field dependence of the energy levels for an axially symmetric $S = \frac{3}{2}$ system with Hamiltonian $\hat{H}$ given by Eq. [3]. The magnetic field $\mathbf{B}$ is set at an angle of 29.4° with the z axis, and we have taken $D = -5.747$ GHz $= -0.191699$ cm^{-1} and $g_{\parallel} = g_{\perp} = g = 1.9858$. This is a case discussed by Pilbrow *et al.* (*3*) for Cr^{3+} transitions in a ruby single crystal. The inset shows the dependence on magnetic field of the energy separation (in cm^{-1}) of the Levels 2 and 4 in the looping transition discussed in the text, observed experimentally at 9.521 GHz $= 0.317586$ cm^{-1}. Note that the $2 \rightarrow 4$ looping transition is created by an avoided crossing between Levels 2 and 3.

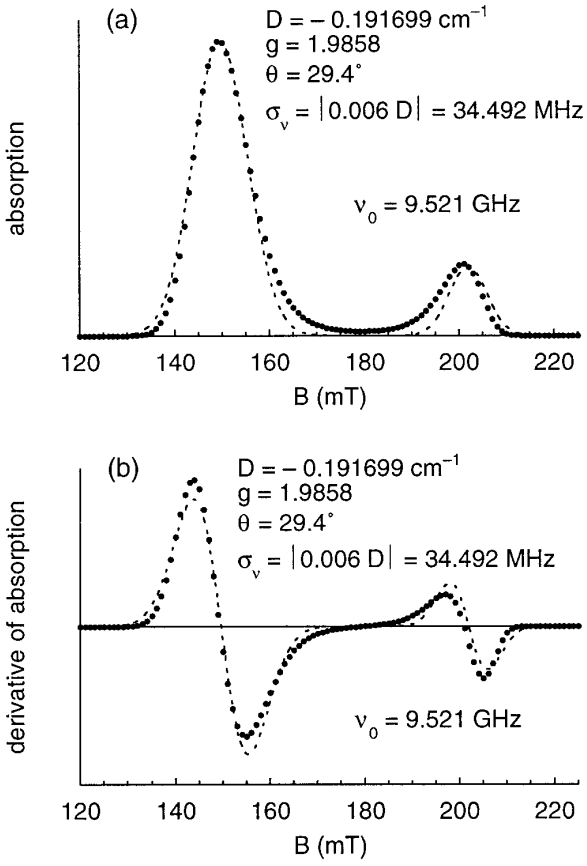

FIG. 3. Exact and approximate calculations of spectra are compared for the *X*-band (9.521 GHz) transitions between Levels 2 and 4 shown in Fig. 2, a case taken from Pilbrow *et al.* (*3*): (a) absorption, (b) derivative of absorption. For the exact calculation, the energy matrix was diagonalized at 1 mT intervals using Eq. [1] (dots). This is compared with the sum-of-the-two-resonances linear approximation (dashed line), for which only two diagonalizations, one at each of the resonance fields, were used. For the dots, the transition probability factor was determined at each field, while for the dashed line only the two probabilities at each of the resonance fields were used. The lineshapes were Gaussian in both cases. For the exact calculation, $\nu(B) - \nu_0$ is substituted directly into the f of Eq. [8], while the sum-of-the-two-resonances linear approximation used Eq. [9]. In both cases σ_ν was $|0.006\ D| = 0.0011502\ \text{cm}^{-1} = 34.482$ MHz. Remaining physical parameters are given in the figure itself.

The approximation (see Ref. (*5*)) that leads to Eq. [2] for a field-swept lineshape results from expanding $\nu(B)$ and $|V_{ij}(B)|^2$ about the resonance field B_0 and keeping just the leading terms,

$$\nu(B) - \nu_0 = (B - B_0)\frac{d\nu(B_0)}{dB_0} + \frac{1}{2}(B - B_0)^2\frac{d^2\nu(B_0)}{dB_0^2} + \cdots, \quad [4]$$

$$\sim (B - B_0)b \quad [5]$$

$$|V_{ij}(B)|^2 = |V_{ij}(B_0)|^2 + \cdots, \quad [6]$$

where

$$b = \frac{d\nu(B_0)}{dB_0} = \frac{1}{h}\frac{d\Delta E(B_0)}{dB_0}. \quad [7]$$

Equation [5] is a *linear approximation* for $\nu(B) - \nu_0$ as a function of B. The inset in Fig. 2 shows the magnetic field dependence of $\nu(B)$ at $\theta = 29.4°$ for a looping transition. The horizontal line at $\nu_0 = 9.521$ GHz intersects the curve at the two resonance fields, 149.646 and 201.961 mT. At these points, the gradients $b = d\nu(B_0)/dB_0$ are -0.0001995 and $0.0002861\ \text{cm}^{-1}/\text{mT}$, respectively. The approximation [4]–[7] has been used recently in simulations of both $S = 2$ (*13*) and $\frac{5}{2}$ (*11*) systems; numerous other references can be found in Ref. (*6*).

To calculate Fig. 3, one needs an explicit lineshape function, $f(\nu - \nu_0, \sigma_\nu)$. While a Lorentzian might be more fundamental, we opted for a Gaussian to mimic (slightly simplified) what Pilbrow *et al.* (*3*) used to fit the ruby spectra. In any event, the nature of f is not paramount to our main point, to be explicated later [approximating $\nu(B) - \nu_0$ by a cubic polynomial in $B - B_0$],

$$f(\nu(B) - \nu_0, \sigma_\nu) = \frac{1}{\sigma_\nu\sqrt{2\pi}}\, e^{-(\nu(B)-\nu_0)^2/2\sigma_\nu^2} \quad [8]$$

$$\sim \frac{1}{|b|(\sigma_\nu/|b|)\sqrt{2\pi}}\, e^{-(B-B_0)^2/2(\sigma_\nu/b)^2}. \quad [9]$$

For the width parameter σ_ν, we took $0.006\ |D|/h$ [$0.0011502\ \text{cm}^{-1} = 34.482$ MHz]—a compromise of the several values used in Ref. (*3*) to fit the experiment.

To calculate the intensity factor $|V_{ij}(B)|^2$,

$$|V_{ij}(B)|^2 = |\langle\psi_i(B)|\mathbf{S}\cdot\mathbf{e}_1|\psi_j(B)\rangle|^2, \quad [10]$$

one must specify the direction $\mathbf{e}_1$ of the microwave field, which is perpendicular to the static field **B,** but not necessarily to the crystal $c(z)$ axis. Pilbrow *et al.* (*3*) took $\mathbf{e}_1$ to be 6° out of the xy plane in their Fig. 2, but here we opted for simplicity and took $\mathbf{e}_1$ to be in the x direction.

In this *first* sample calculation, patterned after Ref. (*3*), the separation of the resonance fields is 52.3 mT, while the left and right half-width-at half-maximum values are $\sqrt{2\ln 2}\,\sigma_\nu/|b| =$ 7.99 and 5.57 mT, respectively. Thus the separation is a little less than 4 times the sum of the half-width values. The sum-of-two-separated-resonances (linear approximation) provides a fair fit in the example shown, but the deviation in the middle region is clearly visible in Fig. 3, as is a shift in the maximum on the right. More pronounced deviations are visible as θ increases, and the resonance fields move closer together, coalesce, and then disappear, as is shown in Fig. 4. Notice that in Fig. 4 the total change in θ is only 1°.

As in Fig. 3, the dots in Fig. 4 represent the spectral response function based on Eq. [1] with a Gaussian (Eq. [8]) for f, and

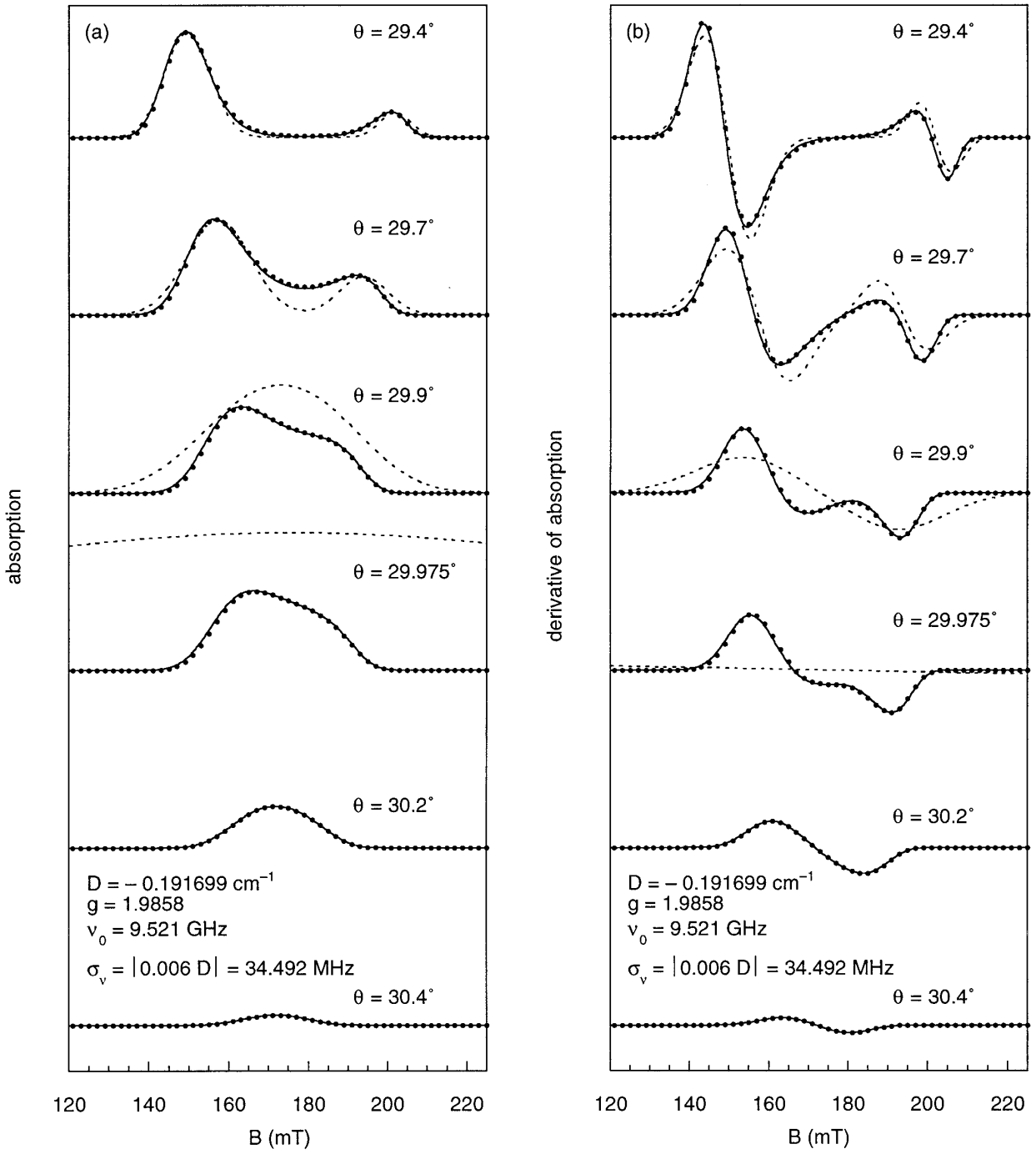

FIG. 4. Exact and approximate calculations of spectra are compared for the *X*-band (9.521 GHz) transitions between Levels 2 and 4 as θ runs from 29.4° to 30.4°: (a) absorption, (b) derivative of absorption. For the exact calculation, the energy matrix was diagonalized at 2 mT intervals using Eq. [1] (dots). This is compared (i) with the sum-of-the-two-resonances linear approximation (dashed line), for $\theta = 29.4°$, 29.7°, 29.9°, and 29.975°, which is just before coalescence at 29.975899 . . .°. Also shown at all values of θ, including two values 30.2° and 30.4° that are past the coalescence angle and for which there are no resonance fields, is (ii) the "cubic approximation" (solid curve that passes through most of the points), in which $\nu(B) - \nu_0$ is approximated by a cubic polynomial in B, and in which the squared transition-dipole factors are approximated by linear interpolation ($\theta = 29.4°$, 29.7°, 29.9°, and 29.975°) or by (for convenience—see text) cubic interpolation ($\theta = 30.2°$ and 30.4°). The lineshapes were Gaussian (Eq. [8]), and σ_ν was $|-0.006\ D| = 0.0011502\ \text{cm}^{-1} = 34.492$ MHz. Remaining parameters are given in the figure itself.

the dashed line represents the sum of two separated resonance contributions using the linear approximation for $\nu(B)$. Notice in particular that at 29.9°, the usual approximation is symmetrical and featureless compared to the true lineshape. At 29.975°, the usual approximation is almost a straight line. In fact, $|b| = |d\nu(B_0)/dB_0|$ is so close to 0, that $e^{-(B-B_0)^2/2(\sigma_\nu/b)^2}$

~ 1, and the spectral response function approaches the constant,

$$S(B_0) \sim 2\,\frac{C'|V_{ij}(B_0)|^2}{\sigma_\nu\sqrt{2\pi}}. \qquad [11]$$

The factor of 2 (cf. Eq. [1] and Eq. [9], the latter with $b = 0$) is from the equal contributions of the two resonances that are coalescing towards the same B_0. This is what is happening at 29.975° in the sum-of-two-separated-resonances linear approximation. Also shown in Fig. 4 via solid lines is the cubic approximation, discussed next.

CUBIC APPROXIMATION NEAR THE LOOPING POINT

We saw in the preceding section that near a looping point the magnetic-field derivative of the transition energy approaches zero, causing the linear-approximation field-swept spectral formula to fail. The crux of the problem is to approximate the curve of $\nu(B) - \nu_0$ vs B, such as is plotted in the inset of Fig. 2. The simplest solution that can also replicate asymmetry is to approximate $\nu(B) - \nu_0$ by a cubic polynomial in B. Recall that the separated-resonance-linear-approximation required two parameters for each resonance: B_0 and $b = d\nu(B_0)/dB_0$. For the two resonances, denote the four parameters by B_{01}, B_{02}, $b_1 = d\nu(B_{01})/dB_{01}$, and $b_2 = d\nu(B_{02})/dB_{02}$. Then there is a unique cubic polynomial in B (Hermite interpolation polynomial) passing through B_{01} and B_{02} with slopes b_1 and b_2, respectively,

$$\nu(B) - \nu_0 \sim (B - B_{01})(B - B_{02})(c_0 + c_1 B) \qquad [12]$$

$$c_0 = -\frac{b_1 B_{02} + b_2 B_{01}}{(B_{01} - B_{02})^2} \qquad [13]$$

$$c_1 = \frac{b_1 + b_2}{(B_{01} - B_{02})^2}. \qquad [14]$$

It is also necessary to model the transition-dipole factor, which changes significantly near the looping point, as is indicated by the asymmetry in intensities in Fig. 3. It turns out that linear interpolation between the values at B_{01} and B_{02} is usually satisfactory and again involves only the two squared-transition-dipole factors already calculated for the separated-resonance-linear-approximation:

$$|V_{ij}(B)|^2 \sim \frac{B - B_{02}}{B_{01} - B_{02}}\,|V_{ij}(B_{01})|^2 + \frac{B - B_{01}}{B_{02} - B_{01}}\,|V_{ij}(B_{02})|^2. \qquad [15]$$

It would not be difficult to improve Eq. [15] to the quadratic or cubic level, if required. The approximation that results from substituting Eqs. [12] and [15] into Eq. [1] is what we refer to as the "cubic approximation" (even though the slower-varying squared-transition-dipole factors are only approximated linearly):

$$S(B) = C'\left[\frac{B - B_{02}}{B_{01} - B_{02}}\,|V_{ij}(B_{01})|^2 + \frac{B - B_{01}}{B_{02} - B_{01}}\,|V_{ij}(B_{02})|^2\right] \times f((B - B_{01})(B - B_{02})(c_0 + c_1 B),\ \sigma_\nu). \qquad [16]$$

The cubic approximation for $\theta = 29.4°$, 29.7°, 29.9°, and 29.975° is plotted in Fig. 4 as an unbroken curve; it passes through each of the "exact" points at the resolution of the figure in this paper.

When θ exceeds 29.9759°, the looping transition is no longer in resonance at any field. Nevertheless, it may still be seen in EMR if the frequency range of its linewidth overlaps the microwave frequency. This is the case in Fig. 4 for $\theta = 30.2°$ and 30.4°. (In Fig. 2 of Ref. (*3*), the 30.4° spectrum is shown experimentally.) It is quite straightforward to calculate such spectra theoretically by continuing to use a cubic approximation to $\nu(B) - \nu_0$; however, formulas different from Eqs. [12]–[16] are required, since there are no resonance fields B_{01} and B_{02}. The procedure we used to obtain the cubic approximations for 30.2° and 30.4° in Fig. 4 was as follows: (i) Pick four B values, B_1, B_2, B_3, and B_4, that are in the vicinity of the looping point. (Here we used 165, 170, 175, and 180 mT.) (ii) Calculate $\nu(B_k)$ and $|V_{ij}(B_k)|^2$ for $k = 1, 2, 3, 4$. (iii) Use the Lagrange interpolation formula to specify cubic polynomials in B that pass through the four computed values respectively. For instance, for $\nu(B)$,

$$\nu(B) \sim \nu(B_1)\,\frac{(B - B_2)(B - B_3)(B - B_4)}{(B_1 - B_2)(B_1 - B_3)(B_1 - B_4)} + \cdots + \nu(B_4)\,\frac{(B - B_1)(B - B_2)(B - B_3)}{(B_4 - B_1)(B_4 - B_2)(B_4 - B_3)}, \qquad [17]$$

and similarly for $|V_{ij}(B)|^2$. It is not necessary to use a cubic vs linear approximation, but because of the four-field nature of the approximation, cubic is the more convenient to implement. (iv) Substitute these cubic approximations into Eq. [1]. The agreement in Fig. 4 at 30.2° and 30.4° is excellent.

Note that if the Boltzmann factor for the transition,

$$[e^{-E_4(B)/kT} - e^{-E_2(B)/kT}]/\sum_{i=1}^{4} e^{-E_i(B)/kT} \qquad [18]$$

depends significantly on B in the region of the spectrum, then it can be incorporated into the cubic approximation by multiplying it into the $|V_{ij}(B)|^2$ factor before fitting the latter.

We remark in passing that Pilbrow *et al.* (*3*) used Chebyshev polynomials to fit the field variation of both the

separation of energies and the transition probabilities, but apparently primarily as an aid in computing the derivatives with respect to field.

CONTRIBUTION OF A LOOPING TRANSITION WITHIN A POWDER SPECTRUM ($S = \frac{5}{2}$, NON-AXIAL CASE)

The zero-field splitting of magnetic energy levels for ferric transferrin ($D \sim 0.25$ cm^{-1}) (*14, 15*) is on the order of the X-band quantum ($v/c \sim 0.3$ cm^{-1}). As a result, there are significant contributions to the observed EMR signals from transitions between pairs of levels that are not degenerate at zero magnetic field (*9, 11*). The X-band experimental spectra of transferrin oxalate provide a clear example of significant absorption from a looping transition involving Levels 2 and 3 (numbered from lowest in energy to highest) of a non-axially symmetric, $S = \frac{5}{2}$ spin system, the Hamiltonian for which to second order is given by Eq. [19].

$$\hat{H} = g\beta\mathbf{B}\cdot\mathbf{S} + D(S_z^2 - \tfrac{1}{3}\mathbf{S}^2) + E(S_x^2 - S_y^2). \qquad [19]$$

The experimental EMR spectra of transferrin oxalate can be approximately simulated in calculations that employ a distribution in zero-field splitting parameters (*11*). Further, the details of the experimental spectra are sensitive to salt and glycerol content of the buffers. For the present discussion, we choose a *single set* of parameters that is within the range of those characteristic of the transferrin oxalate spectra: $g = 2.0023$; $D = 0.27$ cm^{-1}; $E/D = 0.06$.

At fixed angles between the molecule and the magnetic field, the energy levels at zero field are twofold degenerate (Kramers doublets), while at high field they are dominated by the Zeeman term ($g\beta Bm_s$) and split linearly. (For large B, the m_s is asymptotically a good quantum number.) The energy-level diagram and the transitions that contribute to the EMR spectra at 9.23 GHz at fixed angles $\theta = 49°$, $\phi = 46.5°$, chosen to typify a looping transition where the looping property is crucial, are illustrated in Fig. 5. The standard linear approximation $v(B) - v_0 \sim (B - B_0)b$, Eq. [5], is appropriate only if $b = (dE/dB)/h$ is constant across the lineshape. Inspection of Figure 5 reveals that where the 2-to-3 (dotted) curve intersects the horizontal line at 9.23 GHz (208 and 222 mT), not only is dE/dB not constant, but it changes sign within a linewidth.

The contribution of the $2 \rightarrow 3$ transition to the EMR spectrum can be accurately simulated by fitting $v(B) - v_0$ to a cubic polynomial in B, Eqs. [12]–[16], but it is very poorly simulated by the sum-of-two-separated-resonances-linear-approximation of Eqs. [5] and [9], as illustrated in Fig. 6, with a Gaussian lineshape function and frequency width parameter $\sigma_v = 150$ MHz. Note how the cubic fit is almost indistinguishable from the exact frequencies, and note how the slope dv/dB changes dramatically from negative to positive within the 150 MHz linewidth. The two linear approximations of $v(B)$ at the resonance fields fit the exact $v(B)$ only for a tiny fraction of the linewidth region. The spectrum calculated using a Gaussian lineshape function, Eq. [8], is much too broad and intense, and it is without the central structure when the sum-of-separated-resonances-linear-approximation is used.

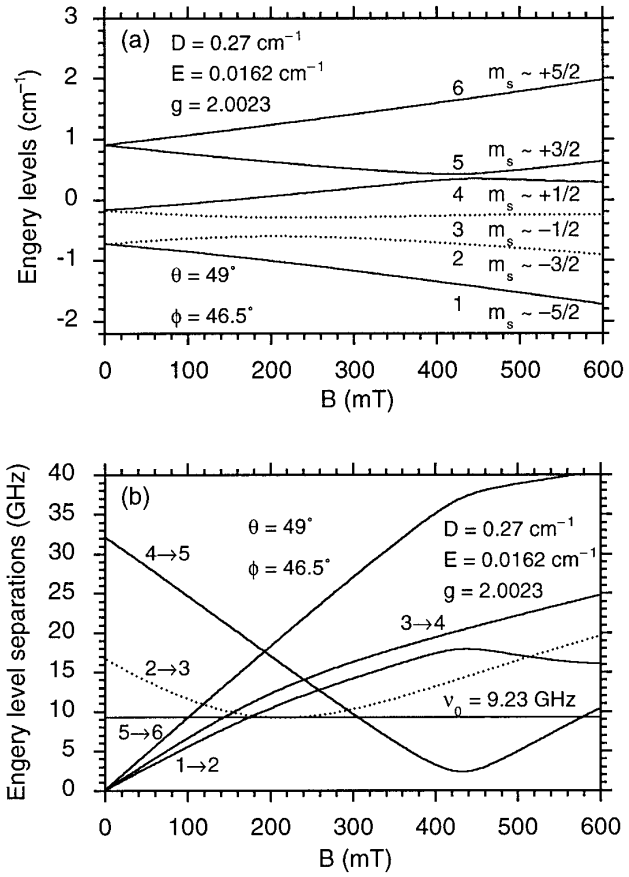

FIG. 5. Typical oriented-molecule energy levels for the $S = \frac{5}{2}$ transferrin system where the two occurrences of a looping transition are within a linewidth. Here the magnetic field makes angles (θ, ϕ) = (49°, 46.5°) with the molecular axes. The spin-Hamiltonian parameters are given on the plot. (a) Magnetic field dependence of the energy levels. The high-field asymptotic m_s values are given on the right. At low and moderate fields, m_s is not a good quantum number, and it is convenient to label the states serially in order of increasing energy. Levels 2 and 3 have been indicated by dotted lines. (b) The field dependence of the six transition-energy differences (in GHz) that contribute significant spectral amplitudes to the final spectrum. The three curves emanating from the origin are the splittings of the Kramers doublets. The other two curves are interdoublet transitions, as labeled. The $2 \rightarrow 3$ transition, our primary interest here, is indicated by a dotted line. A horizontal line has been drawn at the experimental microwave frequency, 9.23 GHz.

At selected angles the sum-of-two-separated-resonances linear approximation fails. But powder spectra result from an average over angles, and looping transitions are strongly angle-dependent. Moreover, the contribution of the looping transition may be "diluted" by contributions from other

transitions. So the question arises: How much does angle-averaging and dilution mute the near-looping-point contributions to powder spectra, whether calculated accurately or inaccurately?

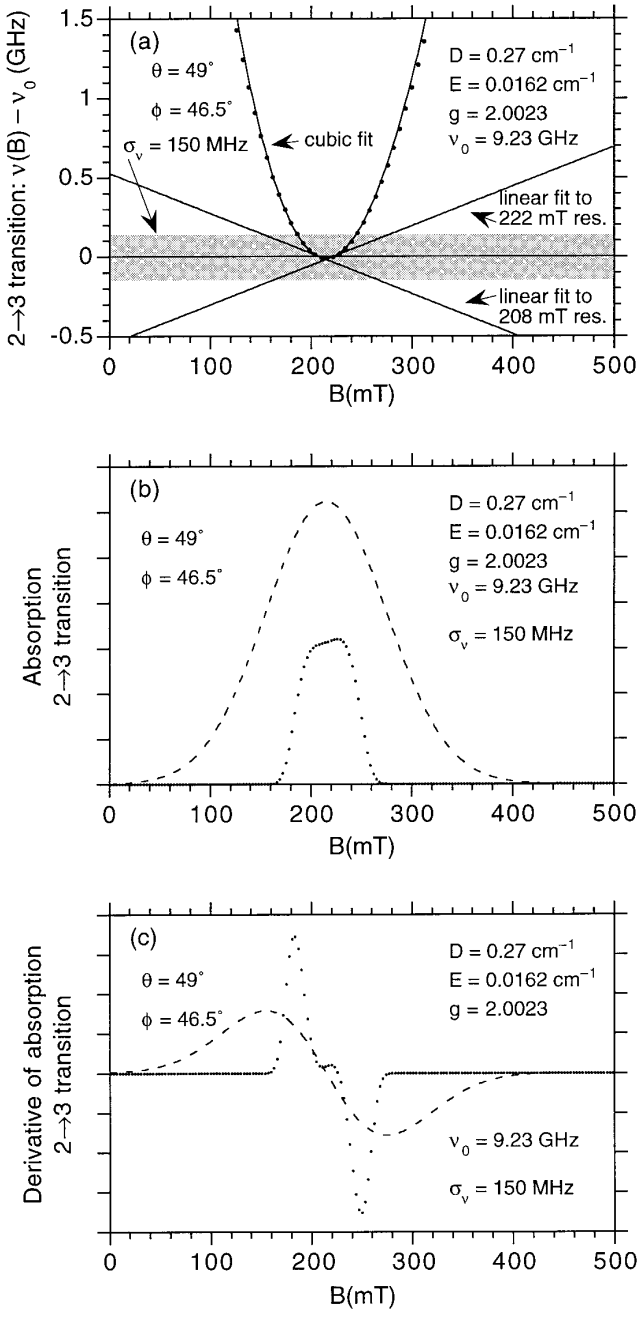

FIG. 6. Simulation of the $2 \rightarrow 3$ looping transition when the magnetic field is at angles $(\theta, \phi) = (49°, 46.5°)$. In this overlapping case, the cubic approximation gives an excellent fit, while the linear approximation is too broad, too intense, and without trace of the central structure. (a) Linear and cubic fits (solid lines) to the "transition frequency minus microwave frequency" (dots). The shaded area is bounded by $\pm\sigma_\nu = \pm 0.15$ GHz, the frequency width parameter. (b) Absorption contribution using a Gaussian lineshape function, Eq. [8], with frequency width parameter $\sigma_\nu = 0.15$ GHz. Dashed line, sum-of-two-separated-resonances linear approximation, Eq. [9]; dots, exact and cubic approximation (which are indistinguishable on this plot), Eqs. [8] and [16]. (c) Derivative of absorption.

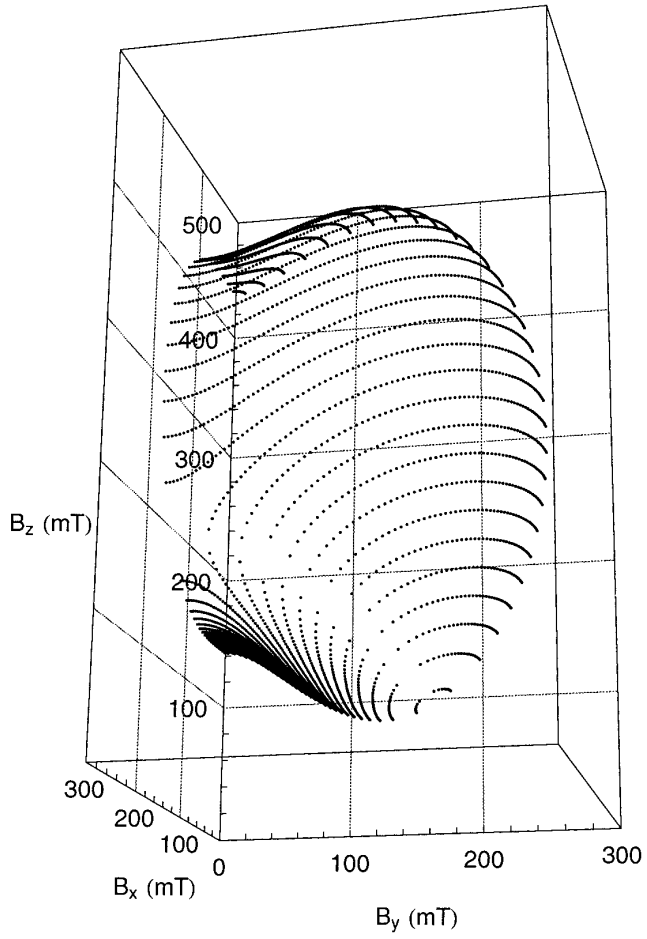

FIG. 7. Resonance fields for the $2 \rightarrow 3$ looping transition form a surface in **B** space. The contours are for constant θ, which runs from 1° to 59° in steps of 2°. For each value of θ, the angle ϕ runs from 90° to 0° in 1° steps, or to the smallest value at which there is still a resonance. For $\theta \leq 35°$, the trajectories emerge from the B_xB_z plane; for $\theta \geq 39°$, the trajectories are loops. For each loop, the looping point falls in the gap of white space (at a non-integer value of ϕ) where the magnetic field vector from the origin is tangent to the surface.

Towards an answer, we first consider the distribution of resonance fields with respect to angle. More complicated than the cylindrically symmetric ruby case of Fig. 1, the resonance fields depend on two angles, and the analogous plot requires three dimensions. In Fig. 7, the resonance fields for the $2 \rightarrow 3$ transition are plotted in 3 dimensions vs the magnetic field (B_x, B_y, B_z). Because of symmetry, a single octant suffices. The resonance fields map out the surface of a solid. Fixed angles for the magnetic field correspond to a ray from the origin. In general, a ray intersects the solid at two points, the two partners of the looping transition. The figure has been generated by taking θ values every 2 degrees, starting with $\theta = 1°$ and ending with $\theta = 59°$. For each value of θ, ϕ decreases in 1° steps from 90° to 0° or to

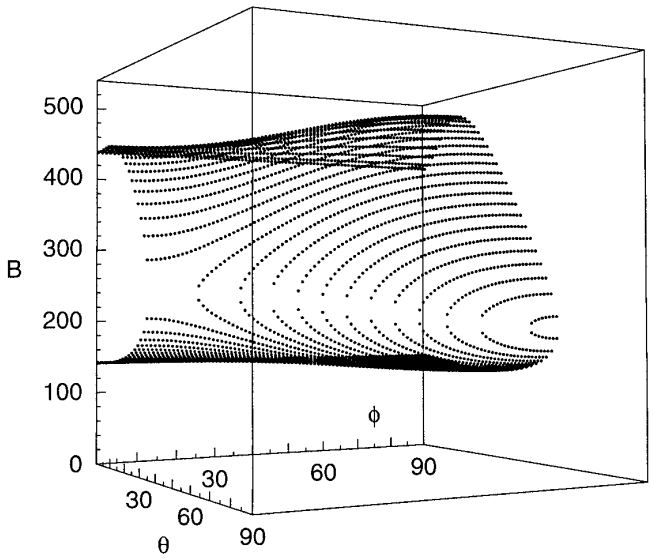

FIG. 8. Resonance field for the 2 → 3 looping transition vs θ and ϕ. B is in mT.

the smallest value in the sequence for which there is still a resonance field. The dots for sequential ϕ values are much closer together than for sequential θ values, so that the "trajectories" for constant θ give the appearance of contour lines. In Fig. 7, the $\theta \leq 35°$ trajectories emerge perpendicularly from the B_xB_z plane, which is vertical and to the left, while those for $\theta \geq 37°$ form closed loops. The tightest loop has $\theta = 59°$ and is towards the lower right. For each of these loops, there are minimum ϕ values below which there are no resonance fields. When a ray from the origin is tangent to the surface, there is a single looping-point resonance field. In Fig. 7, these tangent points occur where the density of points is smallest and would lie in the gaps of white space in the closed curves (delineated by dots at integer values of ϕ). Since the most pronounced features of the powder spectrum occur where the density of points is greatest, one can infer from Fig. 7 that the looping-point contributions will not be dramatic.

In Fig. 8 the same information is plotted as resonance field strength vs θ and ϕ. From this plot one can infer that the z direction contributes a strongest feature around 140 mT and a less strong feature near 440 mT. The highest field contribution is near 500 mT and corresponds to **B** pointing in a certain direction in the yz plane.

In addition to these three-dimensional plots, there are two two-dimensional plots that we have used previously (*1, 11*) that consist of the projections of Fig. 8 onto the $B\theta$ and $B\phi$ planes. These portray the same information as Fig. 8, but make it easier to see certain features. Figure 9 displays θ vs resonance field and shows that the minimum field has θ near 39°, while the maximum field has θ near 13°. Figure 10 plots ϕ vs resonance field and shows that both the minimum and maximum fields have $\phi = 90°$. Both Figs. 9 and 10 show the

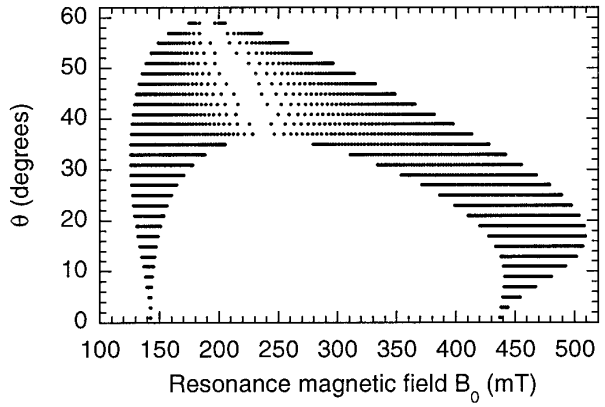

FIG. 9. Resonance field for the 2 → 3 looping transition, θ vs B_0.

buildup of resonances, and consequently sharp features, when B is near 140 and 440 mT; the dominating contributions correspond to **B** pointing close to the polar direction. Both figures also show that the looping-points contribute to the region from 180 to 240 mT.

The contribution from each orientation is determined not only by the resonance field, but also by the intensity and derivative $dv(B_0)/dB_0$. Figure 11 shows the intensity factor $\sin\theta|V_{23}(B_0)|^2$ (Eq. [10]) as a function of the resonance field, and Fig. 12 shows $dv(B_0)/dB_0$ (Eq. [7]). Larger intensity factormeans larger contribution, while greater $|dv(B_0)/dB_0|$ means sharper but weaker contribution (Eq. [9]).

The contribution of the 2 → 3 looping transition to the powder spectrum is simulated in Fig. 13 by summing over an isotropic distribution of angles. The cubic fit (solid line) vs the sum-of-two-separated-resonances-linear-approximation (dashed line) makes a quantitative but not qualitative difference of at most about 10% to the absorption spectrum. The physical parameters are as given in Fig. 5, and the lineshape is Gaussian, Eq. [8], with $\sigma_v = 150$ MHz.

The 2 → 3 looping transition is one of five transitions (of 15 total, see Fig. 5) that contribute significantly to the powder

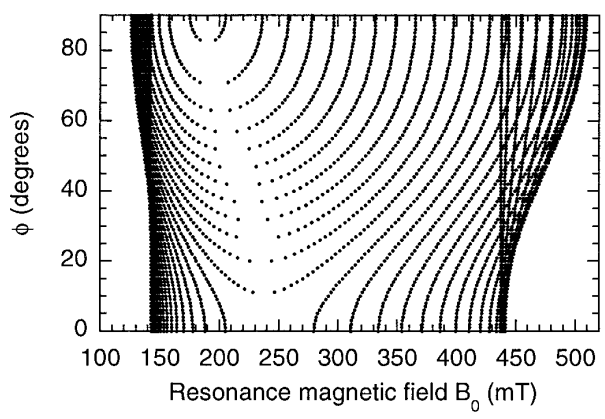

FIG. 10. Resonance field for the 2 → 3 looping transition, ϕ vs B_0.

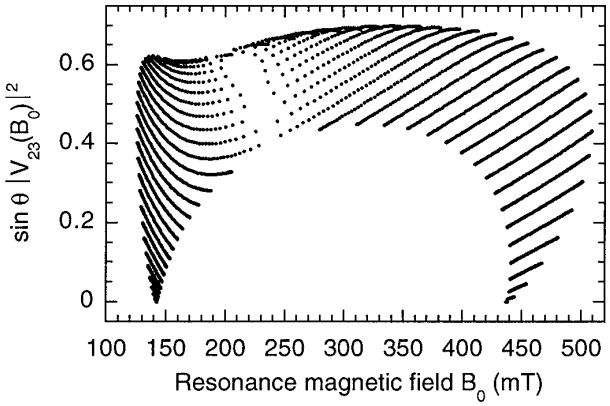

FIG. 11. Resonance field for the $2 \rightarrow 3$ looping transition, intensity factor $\sin\theta|V_{23}(B_0)|^2$ vs B_0.

spectrum. The other four transitions are accurately simulated by the linear approximation. The total simulated spectra are shown in Fig. 14. The solid line is for the case that the $2 \rightarrow 3$ looping transition is done by cubic fit, whereas the dashed line is for the case that the $2 \rightarrow 3$ (as well as the four other transitions in both cases) is fit by linear approximation. After taking an isotropic distribution over angle, the differences between cubic and linear approximations are quantitative, but not qualitative, with maximum difference in absorption about 10% at any point.

CONCLUSIONS

This analysis has employed cubic fits to the non-linear regions of energy level separations involved in magnetic resonance transitions. It provides a convenient and efficient method of calculating field-swept EMR spectra that employs four constants that would be calculated regardless of whether the energy separation is linear or non-linear: the two resonance fields for a "looping" transition and the two gradients $dv(B)/dB$ at the resonance fields. Efficient computation methods become particularly important when simulations of the isotropic distributions of spins are attempted. The transition-probability factors vs magnetic field in the examples presented here have been fit by linear extrapolation between the values at the two resonance fields because (i) linear appears to be sufficient, and (ii) the two values needed for a linear fit are automatically produced when the resonance fields are calculated. (An exception is the "grazing resonance" case treated in Fig. 4.) As pointed out in Ref. (*3*), there may be examples where there is strongly non-linear variation of transition probability or of linewidth over a transition. In such cases, the method outlined here could be generalized to include these other variables.

For the explicit case of transferrin oxalate, cubic fit to the energy separation of the looping $2 \rightarrow 3$ transition is crucial at

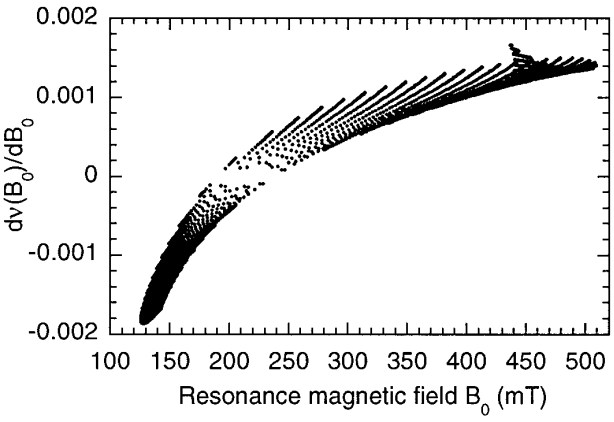

FIG. 12. Resonance field for the $2 \rightarrow 3$ looping transition, $dv(B_0)/dB_0$ vs B_0.

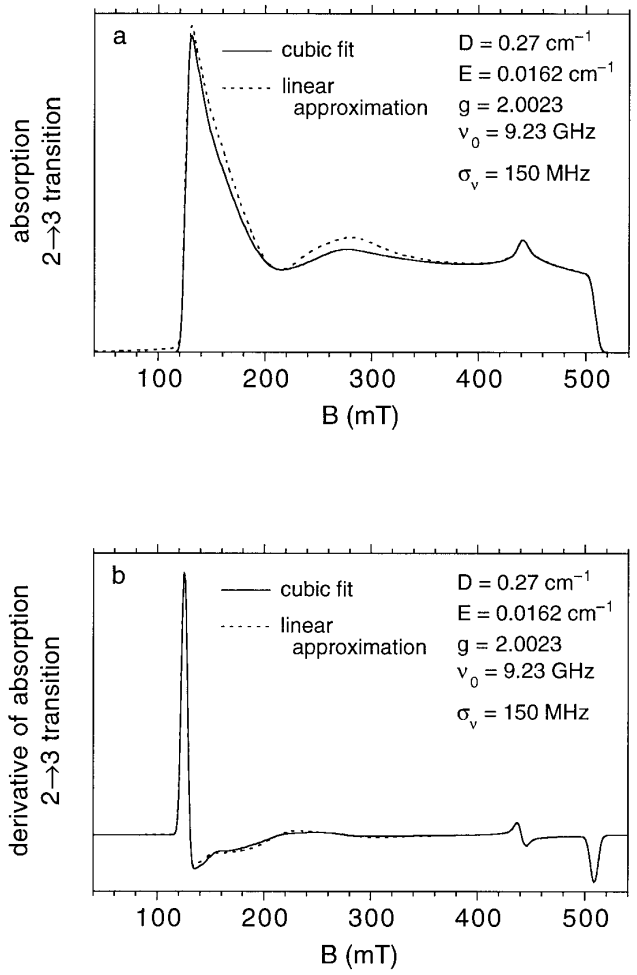

FIG. 13. Contribution of the $2 \rightarrow 3$ looping transition to the powder spectrum by cubic fit (solid line) and by sum-of-two-separated-resonances-linear-approximation (dashed line). Cubic fit makes a quantitative but not qualitative difference of at most about 10% at any point in the absorption spectrum. Physical parameters are given on the figure; Gaussian lineshape, Eq. [8], with $\sigma_\nu = 150$ MHz.

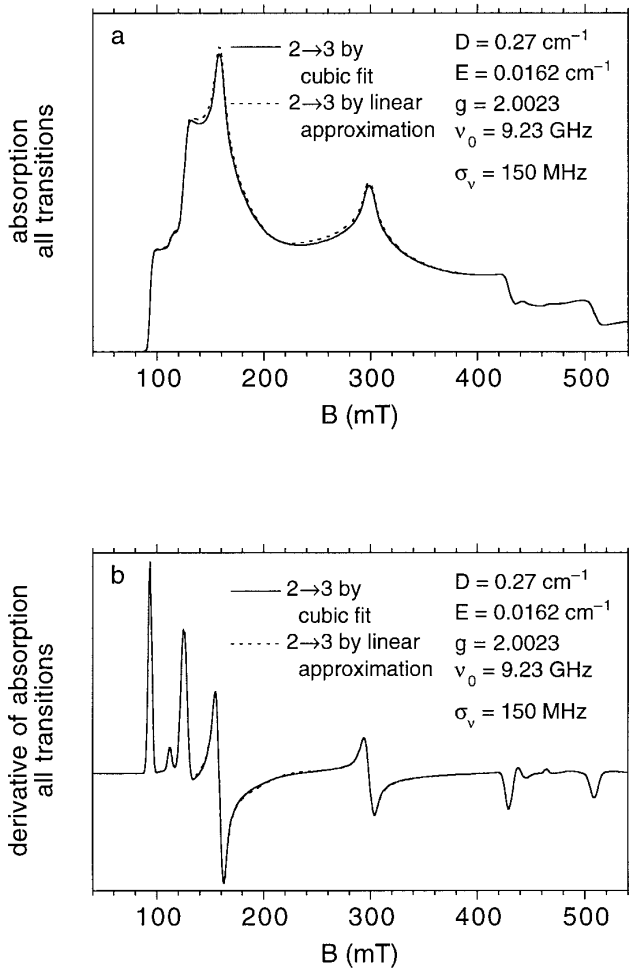

FIG. 14. Calculated spectrum as sum of all significant transitions between the levels of the $S = \frac{5}{2}$ transferrin system for an isotropic distribution of spins, with parameters shown and with Gaussian lineshape (Eq. [8], with $\sigma_\nu = 150$ MHz). Contribution of the $2 \rightarrow 3$ looping transition to the powder spectrum is by cubic fit (solid line) and by linear approximation (dashed line); all other transitions by linear approximation. (a) Absorption; (b) derivative of absorption.

selected angles. But in the isotropic average of a powder spectrum and subsequent dilution from contributions of other transitions in the same spectral region, it produces quantitative but not so dramatic improvement over the usual sum-of-separated-resonances-linear-approximation.

ACKNOWLEDGMENT

This work was supported in part by Grant GM 36232 (to B.J.G.) from the National Institutes of Health.

REFERENCES

1. B. J. Gaffney and H. J. Silverstone, Simulation of the EMR spectra of high-spin iron in proteins, *in* "Biological Magnetic Resonance" (L. J. Berliner and J. Reuben, Eds.), Vol. 13, pp. 1–57 (1993).
2. H. J. Silverstone, disk accompanying volume, *in* "Biological Magnetic Resonance" (L. J. Berliner and J. Reuben, Eds.), Vol. 13, pp. 1–57 (1993). [A more platform-independent version of the two FORTRAN programs on this diskette, with correction of a minor bug in speGIron.f, can be obtained by e-mail on request to HJSilverstone@jhu.edu]. A UNIX version which allows distributions in D or E is available from B. Gaffney (bgaffney@magnet.fsu.edu).
3. J. R. Pilbrow, G. R. Sinclair, D. R. Hutton, and G. J. Troup, Asymmetric lines in field-swept EPR: Cr^{3+} looping transitions in ruby, *J. Magn. Reson.* **52,** 386–399 (1983).
4. D. M. Wang and J. R. Pilbrow, Symmetry relationships for the four energy levels and the angular property of the EPR spectra for a spin-$\frac{3}{2}$ system, *J. Magn. Reson.* **77,** 411–423 (1988).
5. R. Aasa and T. Vänngard, EPR signal intensity and powder shapes: A reexamination, *J. Magn. Reson.* **19,** 308–315 (1975).
6. J. R. Pilbrow, "Transition Ion Electron Paramagnetic Resonance," Clarendon, Oxford (1990).
7. J. Minge, M. J. Mombourquette and J. A. Weil, EPR study of Fe^{+3} in α-quartz: The sodium-compensated center, *Phys. Rev. B* **42,** 33–36 (1990).
8. D. Choi and J. A. Weil, EPR study of Fe^{+3} in α-quartz: Further lithium compensated centers, *Phys. Rev. B* **42,** 9759–9765 (1990).
9. D. M. Wang, D. R. Hutton, and J. R. Pilbrow, Room temperature EPR of $Cr(CN)_6^{-3}$ ions doped into KCl single crystals, *J. Phys. C* **19,** 789–797 (1986).
10. R. Aasa, Powder line shapes in the electron paramagnetic resonance spectra of high spin ferric complexes, *J. Chem. Phys.* **52,** 3919–3930 (1970).
11. K. S. Doctor, B. J. Gaffney, G. Alvarez, and H. J. Silverstone, EPR spectroscopy of interdoublet transitions in high-spin iron: Applications to transferrin oxalate, *J. Phys. Chem.* **97,** 3028–3033 (1993).
12. K. S. Doctor and B. J. Gaffney, High frequency EPR predictions for the non-heme iron protein lipoxygenase, *Appl. Magn. Reson.* **11,** 425–435 (1996).
13. M. P. Hendrich and P. G. Debrunner, Integer-spin electron paramagnetic resonance of iron proteins, *Biophys. J.* **56,** 489–506 (1989).
14. J. Dubach, B. J. Gaffney, K. More, G. R. Eaton, and S. Eaton, The effect of the synergistic anion on EPR spectra of iron-transferrin anion complexes is consistent with bidentate binding of the anion, *Biophys. J.* **59,** 1091–1100 (1991).
15. S. A. Kretchmar, M. Teixeira, B.-H. Huynh, and K. N. Raymond, Mössbauer studies of electrophoretically purified monoferric and diferric human transferrin, *Biol. Metals* **1,** 26–32 (1988).